Journal of Materials and Environmental Science
ISSN : 2028-2508
e-ISSN : 2737-890X
CODEN : JMESCN

J. Mater. Environ. Sci., 2024, Volume 15, Issue 1, Page 116-135

http://www.jmaterenvironsci.com

Equilibrium and Thermodynamic Studies on Biosorption of Pb (II) and Cd (II) Ions from Wastewater onto Clay Cellulose Nanocomposite Adsorbent

Kinoti I. K. [1] *, Marangu J. M. [1], M'thiruaine C. M. [1]

[1]*Department of Physical Sciences, Meru University of Science and Technology, Meru, Kenya*

[*]*Correspondence author Email: ismaelkinoti95@gmail.com*

Received *24 Dec 2023,*
Revised *16 Jan 2023,*
Accepted *18 Jan 2023*

Keywords:
- ✓ *Cellulose*
- ✓ *Clay*
- ✓ *Heavy Metals*
- ✓ *Isotherms*
- ✓ *Nanocomposites*
- ✓ *Water Hyacinth*

Citation*: Kinoti I. K., Marangu J. M., M'thiruaine C. M. (2024) Equilibrium and Thermodynamic Studies on Biosorption of Pb (II) and Cd (II) Ions from Wastewater onto Clay Cellulose Nanocomposite Adsorbent, J. Mater. Environ. Sci., 15(1), 116-135*

Abstract: The adsorption of lead (II) and cadmium (II) ions from aqueous solutions by novel water hyacinth-based cellulose clay nanocomposite were studied and their adsorption performance established using the Langmuir, Dubinim-Radushkevich, Temkin and Freundlich isotherm models. The water hyacinth-based cellulose clay nanocomposite (CCNC) was synthesized by solution blending method, with poly vinyl alcohol solution as the dispersion medium. Characterization of the CCNC was done using Fourier Transform Infrared Spectroscopy (FTIR) and Scanning Electron Microscopy (SEM). According to the adsorption studies, Pb (II) ions were adsorbed by the CCNC material through a heterogeneous process, whereas Cd (II) was adsorbed through both monolayer and heterogeneous processes. While Freundlich and D-R isotherms were the best at explaining the adsorption of Pb (II), Langmuir, Temkin, and Freundlich isotherm models were most effective at explaining the adsorption of Cd (II). The adsorption process was exothermic, according to thermodynamic analyses. The pH value of 4, the adsorbent dose of 0.8g per 100 ml of contaminated water, the temperature of 25 °C, and the contact period of 30 to 120 minutes were shown to be the most effective conditions for the adsorption of Pb (II) and Cd (II) ions from wastewater. The highest percentage metal ion removal was observed to be 99.6 % (Cd^{2+}) and 99.9 % (Pb^{2+}).

1. Introduction

Over the past 100 years, water use has increased by a factor of about 6, growing consistently at a rate of about 1% per year (UN-Water, 2018). This is attributed to rapid population growth, urbanization, changing climate, and shifting patterns of water consumption. This consequently has led to an acute increase in wastewater production. With a consistent growth of approximately 3.4 % in urbanization and industrialization, especially in developing countries, it can only mean water contamination will increase (Kuwonu, 2017; Razzouki *et al.*, 2015). Additionally, flooding and high precipitation due to climate change, have been linked to high heavy metal concentrations. If efficient methods to reclaim, reuse and recycle water are not utilized, it is estimated that the world will face 40% water deficiency by 2030 (Malone, 2016).

According to the United Nations World Water Development Report (UN Water, 2021), more than 80% of wastewater produced in developing countries is released back to the environment in untreated form. With contaminants ranging from organic biodegradable compounds to inorganic toxic compounds such as heavy metals, the dangers citizens of such countries are exposed to, are of concern. Heavy metals are particularly high-risk contaminants owing to their ability to bioaccumulate. Some of them, such as iron, copper, and manganese, participate in crucial metabolic processes in the human body, including the formation of hemoglobin (Nih, 2022), connective tissues and blood vessels (Nih, 2021), and cholesterol metabolism (Rehman *et al.*, 2018) in trace amounts. At higher concentrations, heavy metals such as cadmium and lead have been reported to play a role in metal-induced carcinogenesis through DNA damage (Azeh Engwa *et al.*, 2019). Spot contaminations for lead and cadmium include municipal, garage, car wash and industrial effluents such as battery manufacture and repair, paint and metal work industries (Njuguna *et al.*, 2017). In developing countries, these sources are centered on urban centers characterized by a high population. According to a 2017 United Nations report, 4 out of 10 people in Africa were living in urban centers (Kuwonu, 2017). With an urbanization growth rate of about 3.4 %, it is possible that half of the population in Africa will be living in urban centers by 2035 (Kuwonu, 2017). This would mean more cars burning fossil fuels, and an increase in carwashes and garages, which would increase heavy metal contamination, if greener solutions are not embraced. Consequently, growth in improved agriculture to cater for the urban population would mean a greater use of agrochemicals, most of which are heavy loaded with toxic heavy metals (Tutic *et al.*, 2015). The housing sector too, in an attempt to shelter the population, would potentially exacerbate heavy metal contamination through paint production and metal manufacture (Apanpa-Qasim *et al.*, 2016; Ogilo *et al.*, 2017; Megertu & Bayissa, 2020). Furthermore, flooding and heavy precipitation have been linked to an increase in heavy metal concentration in urban watercourses (Frogner-Kockum *et al.*, 2020; Iordache *et al.*, 2022). With the current state of climate change predicted to worsen (UNEP, 2020), it is possible to face high concentrations of heavy metal contamination in water bodies, soil and consequently flora and fauna.

Various methods have been studied and utilized to remove heavy metals and other contaminants from wastewater with a goal for reuse in irrigation, human and animal consumption, among other activities. Use of activated carbon (D. Saha & Grappe, 2017), reverse osmosis (Karunakaran *et al.*, 2021), ultrafiltration (Aloulou *et al.*, 2020) and electrodialysis (Juve *et al.*, 2022) are highly effective methods in the removal of heavy metals. However, developing countries cannot sustain the extensive use of these methods in relation to high costs of setting up, maintenance, and the technology required to run them (Marshall, 2017; Nelligan *et al.*, 2011). Low-cost adsorptive alternatives have recently been of interest because of their efficiency and selectivity in the removal of wastewater contaminants such as heavy metals. Such a low-cost material is clay. Clay and clay minerals have been used in adsorption of various water contaminants such as heavy metals (Sdiri *et al.*, 2011), cationic dyes (El Kassimi *et al.*, 2021) and pharmaceuticals (Arya & Materials, 2016).

Clay can be defined as soil with particle size falling below 0.005mm; or a rock, made up of clay particles; that shows plasticity when wet and coherence when dry (Daumier *et al.*, 2020). Such a rock is made up of varying percentages of clay minerals such as kaolinite, mica, and illite, among others. Clay minerals are usually phyllosilicates, made up of layered tetrahedral silica and octahedral aluminium, magnesium, or iron sheets, classifiable through their structural arrangements (Gu *et al.*, 2019). The tetrahedral structures usually have a Si atom surrounded by four hydroxyl groups while the octahedral structure has an Al, Mg or Fe atom surrounded by six hydroxyl or oxygen atoms. These two layers can be arranged in the ratio 1:1 as in kaolinite, 2:1 as in smectites, illite and mica or mixed as

2:1:1 as in chlorite (Gu *et al.*, 2019). Clay properties such as high cation exchange capacity, abundance and high surface area, has had them utilized as heavy metal adsorbents for wastewater decontamination (Hızal & Yılmazoğlu, 2021). Functional groups and surface charges available to the clay minerals are responsible for the heavy metal removal, especially in acidic environments (Gu *et al.*, 2019).

In adsorptive studies, clay minerals (Azzaoui et al 2016) are good heavy metal adsorbents, but achieve low metal ion removal especially in the presence of competing ions (Jiang *et al.*, 2010). To improve their adsorption, researchers have resulted to modification techniques that either improve active adsorptive sites or make the material ion specific (Kennedy *et al.*, 2018). Such a modifier, which is commonly utilized in response to being abundant in natural environment, is cellulose. When extracted from plants, unmodified cellulose exhibits low metal ion adsorption due to low specific surface area (Suhas *et al.*, 2016). Therefore, it is utilized in modified form or as a precursor for other heavy metal adsorbents, to enhance removal (El-Aziz *et al.*, 2018). Modifying clay with cellulose (to form a nanocomposite) improves the surface area of the clay for heavy metal adsorption and thus enhances removal (Kumar *et al.*, 2012).

Nanocomposite materials are multiphase materials containing at least one dimension less than 100 nm, or the composite phase have distances within the nanoscale between them (Neitzel *et al.*, 2012). Such materials exhibit advanced capabilities due to enhanced specific surface area to volume ratio, which in the field of water treatment, is indispensable. Nanocomposite materials are particularly applied in water decontamination in relation to very high removal capacities, ease of regeneration, low-cost fabrication, ease of modification and high selectivity in adsorbate removal. In heavy metal removal different researchers have applied various modifications to clays, enhancing them at the nanoscale, to achieve high removal capacities. (Soltani *et al.* (2019) used polyaniline clay hybrid material in the removal of Cu (II) and reported a high removal capacity of about 22.7 mg/g with just 0.05 g of the material. Zhang & Wang (2015) used lignocellulosic montmorillonite nanocomposite in the adsorptive removal of Ni (II) ions reporting a maximum adsorption capacity of 94.86 mg/g. Tirtom *et al.* (2012) used epichlorohydrin crosslinked chitosan clay composite beads in the comparative removal of Ni (II) and Cd (II) ions from aqueous solutions, reporting adsorptive capacity of 32.36 mg/g and 72.31 mg/g respectively. However, low-cost adsorbents, inclusive of clay-based nanocomposites have only been studied against low metal ions concentrations. There is a gap in the performance of these adsorbents in the removal of heavy metals in relatively high metal ion concentrations. In this paper we report on utilization of the clay cellulose nanocomposite in the adsorption of high concentration Cd (II) and Pb (II) ions from contaminated water (Aaddouz; et al; 2023). The adsorption parameters, isotherms, characterization, and thermodynamic studies are also discussed.

2. Methodology

2.1 Materials

The cellulose used in the research was isolated from water hyacinth (*Eichhornia crassipes*) that was collected from Lake Naivasha (-0.81247, 36.29464), Kenya. The clay used in the study was collected from Meru (0.13166, 37.71257), Kenya. The chemicals used in the study were analytical grade and were used without further purification. In the study, the shaking water bath model SHA-C, the analytical balance model MA2104C, the magnetic stirrer and hotplate model MS/-H550-S, a scanning electron microscope model Hitachi S-3400N, the Fourier Transform Infrared Spectroscopy (FTIR) model IRTRacer-100 and the Shimadzu Atomic Absorption Spectroscopy (AAS) model AA-7000 with an autosampler model ASC-7000 were used.

2.2 Methods

2.2.1 Isolation of Cellulose

The cellulose was isolated following the method of Istirokhatun *et al.* (2015). Water hyacinth (WH) samples were washed, roots were removed, and the stems and leaves cut to small pieces. Then they were sundried for 12 hours and oven-dried overnight at 100 °C. The samples were then blended. 40 g of WH powder was extracted using 2:1 toluene: ethanol solution for 3 hours. They were then bleached with a 3 % NaOCl solution at 80 °C for 2 hours, followed by hydrolysis with 1 % NaOH at 60 °C for another 2 hours. The second bleaching was carried out with 1 % NaOCl at 75 °C for 3 hours while stirring, then 5 % HCl was added to act as a catalyst through acid hydrolysis. The temperature was adjusted to 65 °C and the process continued for 6 more hours. The resultant cellulose was filtered and washed with distilled water to remove the acid.

2.2.2 Synthesis of the Nanocomposite

To synthesize the clay-cellulose nanocomposite, the method by Abunah *et al.*, (2019) was adopted. 2 kg of raw clay was first washed to remove impurities and suspended for 72 hours to drip off water. Then it was converted to sodic form using 1M NaCl. 20 g of polyvinyl alcohol were hydrated for 2 hours at 90 °C in 2 L of distilled water, then sodic clay was added and stirred for 20 minutes. Cellulose was then added while stirring for an additional 20 minutes. The solution was allowed to cool and drained off for 72 hours. The residue was oven dried at 100 °C for 12 hours, ground and sieved through 75-micron sieve before use in adsorption studies.

2.3 Characterization of Samples

FTIR characterization was performed using an FTIR (IRTracer-100) instrument in the 4000-400 cm^{-1} range with a resolution of 1 cm^{-1}, in attenuated total reflectance (ATR) mode. The dried clay and clay-cellulose samples were first ground on hand using a mortar and pestle. The resultant fine powder was placed on the ATR sample holder and the spectrum recorded within the forementioned range.

Electron microscopy technique was used for the characterization of morphology. To prepare powdered sample for the technique, small volumes of 2 - 3mg were dispersed in 200mL ethanol solution in an Eppendorf, that were sonicated for 15 minutes. A silicon wafer held the samples that were dried and then scanned through the SEM. Samples were gold-coated to make them conductive. SEM characterization for both clay and clay-cellulose nanocomposite was done using a scanning electron microscope model Hitachi S-3400N, and the micrographs provided at a magnification of 25 kX.

2.4 Optimization of Experimental Parameters

To determine the optimal parameters of metal ion adsorption, one parameter was variated, while all the others were kept constant. The optimum condition was utilized for a subsequent step. To determine the effect of pH on adsorption, 0.8 g of the nanocomposite was added to 250 ml conical flasks with 30 mg/L metal ion concentration at a pH of 2, 3, 4, 5 and 6. The samples were fixed in a shaking water bath set at 170 rpm and 25 °C and run for 120 minutes. The pH was adjusted using 0.1M NaOH or 0.1M HCl solution. To study the effect of temperature on metal ion adsorption, 0.8 g of nanocomposite was added to water with 30 mg/L of metal ion concentration and temperature studied at 20, 25, 35 and 45 °C in a shaking water bath set at 170 rpm for 120 minutes each. The effect of metal ion concentration was studied at concentrations 10, 20, 30, 50, and 100 mg/L with 0.8 g of the nanocomposite, for 120 minutes. To study the effect of contact time on adsorption, 0.8 g of the nanocomposite was added to 100 ml of 30 mg/L of metal ion solution, pH 4, and run at 170 rpm, shaking water bath 25 °C, reading taken at 10, 20, 30, 60 and 120 minutes. Experiments were conducted in triplicate and mean data was

calculated. To calculate the distribution ratio, adsorption percentage and capacity, **Eqn 1, 2 and 3** respectively, were used (Ostovaritalab & Hayati-Ashtiani, 2019).

$$K_d = \frac{C_i - C_e}{C_e} \times \frac{V}{m} \quad \textbf{Eqn.1}$$

$$\% R = \frac{100 \times K_d}{K_d + \frac{V}{m}} \quad \textbf{Eqn. 2}$$

$$Q_e = K_d \times C_e \quad \textbf{Eqn. 3}$$

Where K_d is distribution ratio, C_i (mg/L) the initial concentration of metal ion concentration, C_e (mg/L) the concentration of metal ions at equilibrium, V the volume of solution in litres, m the mass of the adsorbent in grams, $\% R$ the adsorption percentage and Q_e the adsorption capacity in mg/g.

2.5 Adsorption Studies

To study the adsorption mechanism, the adsorption isotherms and thermodynamics were investigated. To study the adsorption isotherms, five solutions with 20, 30, 50, 100 and 200 mg/L of Pb (II) and Cd (II) ion separately, were prepared. In each 1.4g and 0.8g for of the nanocomposite were added in the Pb (II) and Cd (II) ion solutions respectively. The solutions were placed in the shaking water bath for 120 minutes at room temperature at a speed of 170 rpm. The samples were then filtered, and the metal ion concentrations were determined using AAS. The obtained data was fitted to Langmuir, Dubinim-Radushkevich, Temkin and Freundlich isotherm models. Langmuir isotherm assumes a monolayer adsorption process, typical in a single solute saturated non-linear process (Matouq *et al.*, 2015). The Langmuir non-linear equation is given by **Eqn. 4**.

$$Q_e = \frac{Q_m k_l Ce}{1 + k_l C_l} \quad \textbf{Eqn. 4}$$

And in the linear form in **Eqn. 5**

$$\frac{C_e}{Q_e} = \frac{1}{Q_m} C_e + \frac{1}{k_l Q_m} \quad \textbf{Eqn. 5}$$

Where Q_m and k_l are Langmuir constants representing monolayer adsorption capacity in mg/g and adsorption constant in mg/L respectively. These values were estimated from the gradient and intercept of the plot of $\frac{C_e}{Q_e}$ versus C_e respectively. Kl values relate to the energy released during adsorption and are useful in the estimation of a unitless constant, R_l, through **Eqn. 6** (Inyinbor *et al.*, 2016).

$$R_l = \frac{1}{(1 + k_l C_0)} \quad \textbf{Eqn. 6}$$

When the value of R_l is above 1, the adsorption is unfavorable for fitting with Langmuir, R_l = 1 translates to a linear adsorption, 0 < R_l < 1 tell that the adsorption favorably fitted to Langmuir and if R_l = 0, the adsorption process is irreversible (Hua & Li, 2014).

The Freundlich non-linear isotherm is given in **Eqn. 7** (Ayawei *et al.*, 2017).

$$Q_e = k_f \cdot Ce^{1/n} \quad \textbf{Eqn. 7}$$

In linearized form, Freundlich isotherm becomes **Eqn. 8.**

$$\ln(Q_e) = \ln k_f + \left(\frac{1}{n_f}\right) \ln C_e \quad \textbf{Eqn. 8}$$

Where k_f (L/g) and n_f (unitless) are Freundlich constants estimated by the intercept and gradient of the plot of $\ln(Q_e)$ versus $\ln C_e$.

Freundlich isotherm is applied to non-uniform distribution of heat of adsorption, common on heterogenous surfaces, assuming multilayer adsorption, thereby not limited to monolayer adsorption (Fosso-Kankeu *et al.*, 2017). The nf parameter on Freundlich isotherm indicates the deviation of the adsorption process from linearity and intensity (Mu & Sun, 2019). When the value is close to 0, the adsorption process is more heterogeneous. If below 1, the metal ions are adsorbing by chemisorption. If it is greater than 1, the adsorptive process is cooperative (physisorption) in nature (Foo & Hameed, 2010). A high R^2 value in Freundlich isotherm implies multilayer adsorption of adsorbates.

The Temkin isotherm, given in **Eqn. 9**, ignores extremes of adsorbate concentration to focus on a linear decrease of the heat of adsorption (Inyinbor *et al.*, 2016. Jodeh et al 2018).

$$Q_e = \frac{RT}{b}\ln(\beta C_e) \qquad \textbf{Eqn. 9}$$

The linear form is given in **Eqn. 10**.

$$Q_e = \frac{RT}{b}\ln K_t + \frac{RT}{b}\ln C_e \qquad \textbf{Eqn. 10}$$

Where b (j/mol) and Kt (L/g) represent Temkin constants, calculated from the slope and intercept of the plot of Q_e versus $\ln C_e$ respectively. This isotherm is applicable to adsorption data without a saturation plateau, characterized by Type II, III and V isotherms (Chu, 2021). Temkin isotherm assumes uniform distribution of bonding energy limited by a maximum energy of bonding. The term 'b' in Temkin isotherm is related to the heat of adsorption, whereby a positive value indicates an exothermic process and a negative value, an endothermic process (Altaher, 2016).

The Dubinim-Radushkevich isotherm is given in **Eqn. 11** and **12** in non-linear and linear forms, respectively.

$$Q_e = Q_o \exp(-\beta\varepsilon^2) \qquad \textbf{Eqn. 11}$$

$$\ln Q_e = \ln Q_o - \beta\varepsilon^2 \qquad \textbf{Eqn. 12}$$

Where ε is Polanyi potential, β (mol^2/kJ^2 an activity coefficient that is useful in determination of mean sorption energy, E (kJ/mol), Qo the maximum adsorption capacity in mg/g. ε and E are calculated from the **Eqn. 13** and **14** respectively.

$$\varepsilon = RT\ln\left(1 + \frac{1}{C_e}\right) \qquad \textbf{Eqn. 13}$$

$$E = \frac{1}{\sqrt{2\beta}} \qquad \textbf{Eqn. 14}$$

A plot of ln Qe versus ε^2 is used to calculate the values of ln Qo and β from the intercept and slope, respectively. When the value of E is between 8 – 16 kJ/mol, that implies that the adsorption process proceeds through chemisorption or ion exchange. If the value is below 8 kJ/mol, the adsorption is physisorption (Matouq *et al.*, 2015; Akartasse et al ; 2022).

To evaluate the thermodynamic parameters Gibbs free energy (ΔG^0), enthalpy (ΔH^0) and entropy (ΔS^0) of the Pb (II) and Cd (II) adsorption, **Eqn. 15**, and **16** were used (Yeganeh *et al.*, 2019).

$$\Delta G^0 = -RT\ln k_d \qquad \textbf{Eqn. 15}$$

$$\ln k_d = \frac{-\Delta G^0}{RT} = -\frac{\Delta H^0}{RT} + \frac{\Delta S^0}{R} \qquad \textbf{Eqn. 16}$$

Where R is the universal gas constant, T temperature in Kelvin, and k_d as given previously in **Eqn. 1.**

3. Results and Discussion

3.1 Characterization of Clay and Nanocomposite

3.1.1 Characterization by Infrared Spectroscopy

The clay and clay-cellulose peaks as characterized by Fourier Transform Infrared Spectroscopy are presented in **Figure 1**.

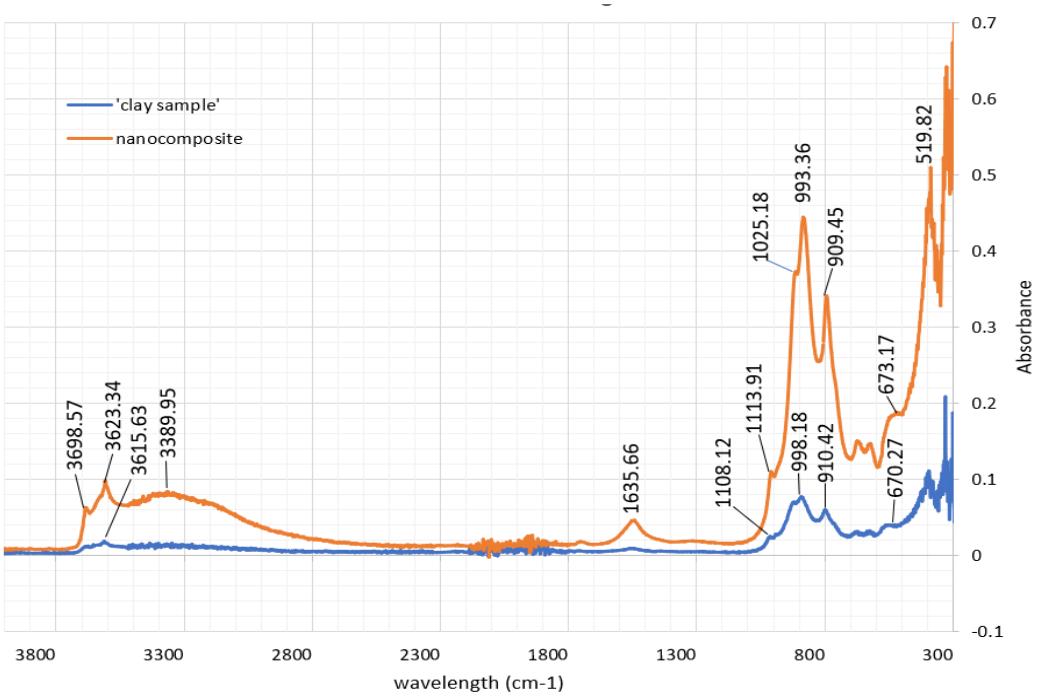

Figure 1: FTIR spectra for clay and cellulose-clay nanocomposite.

Fourier transform infrared spectroscopy (FT-IR) is a technique used intensively to determine the chemical structure of a material by studying the adsorption or transmission of functional groups in IR (Gaffney *et al.*, 2012). Specific functional groups show IR peaks at specific points in the IR spectra and therefore are identifiable through this technique. Generally, IR spectra show bands in distinct regions known as the group frequency region (4000 – 1300 cm^{-1}) and the fingerprint region (1200 - 700 cm^{-1}) (Bruice, 2016). The fingerprint region is the most important region, as most functional groups are detectable in this region. Therefore, it is used in the identification of compounds (Bruice, 2016).

The infrared spectrum of the clay sample (black) showed peaks at 3615.63, 1108.12, 998.18, 910.42, and 670.27 cm^{-1}. The characteristic peak at 3615.63cm^{-1} (νOH) is assigned to stretching vibration of AlOH and MgOH on the structure of the clay (Ashouri *et al.*, 2021; Hayati-Ashtiani, 2012). The peaks at 1108.12 and 670.27 cm^{-1}(νSi-O) are assigned to SiO stretching vibrations in the clay interlayers (Hayati-Ashtiani, 2012; Imam *et al.*, 2020). The peak at 998.18 cm^{-1}(δ Si-O-Mg) corresponds to Si-O-Mg bending vibrations in the internal structure of the clay, indicating a possible substitution of Al^{3+} by Mg^{2+}, which is common in montmorillonite clays. This substitution effect is responsible for high cation exchange capacity and swelling in such clays (Daumier *et al.*, 2020). The peak at 910.42 cm^{-1} (δAl-Al-OH) is assignable to bending vibration of Al-AlOH (Alsawalha *et al.*, 2016). Peaks at 3615.63 cm^{-1} (Al (Mg) -OH), 1108.12 cm^{-1} (Si-O), 998.18 cm^{-1} (Si-O-Mg) and 910.42 cm^{-1} (Al-Al-OH) which are in very close agreement with literature values show the presence of a montmorillonite clay mineral in the sample (Ostovaritalab & Hayati-Ashtiani, 2019; Putro *et al.*, 2017,

El Hammari et al 2022). In research by Alexander *et al.* (2018) investigating the physicochemical characteristics of bentonite clay, the authors reported -OH vibrations due to clay structure and water molecules in the region 3750-3500 cm^{-1}. Characteristic bands of the silicates in the clay were observed in the fingerprint region (1200 – 700 cm^{-1}). Other bands correlating to Si-O and Al-O were observed at 600 – 400 cm^{-1} regions of the IR spectra. Other researchers investigating montmorillonite-based clays reported similar findings (Yildiz *et al.*, 2004; Chashechnikova *et al.*, 2005; Jia *et al.*, 2011; Ostovaritalab & Hayati-Ashtiani, 2019) reported presence of Si-O-Si, Si-O-Al in the region 550-450 cm-1 and Si-O and Al-O bonds in the region 1150 - 1000 cm^{-1}.

When the cellulose structure is introduced into the clay, most bands are shifted and enhanced, as shown in **Figure 3** and **Figure 4**. The clay peak at 3615.63 cm^{-1} is intensified and shifted to 3623.34 cm^{-1}. This shift is related to the effect of -OH functional groups present in the cellulose. New bands in the nanocomposite structure are noticed at 3698.57 and 3389.95 cm^{-1} which correspond to -OH vibrations due to absorption of interlayer water (Yildiz *et al.*, 2004). This was an indication of surface hydration of the nanocomposite with respect to the introduction of cellulose into the structure. In similar research, Chashechnikova *et al.* (2005) reported fairly weak -OH stretching in the region 3500 – 3200 cm^{-1} in organically modified clays, which indicated weak surface hydration of the composite samples based on hydrophobic benzene rings. The nanocomposite also introduces a peak at 1635.66 cm^{-1} representing C=O and C=C vibrations due to cellulose (Ostovaritalab & Hayati-Ashtiani, 2019). The peaks at 3389.95 cm^{-1} and 1635.66 cm^{-1} have been reported before in cellulose studies (Jia *et al.*, 2011). The peaks at 1108.12 and 670.27 cm^{-1}, in the clay sample, were observed to have shifted to 1113.91 and 673.17 cm^{-1} respectively, which indicate a shift in the Si-O bonds with introduction of cellulose structure into clay. It is possible that the Si-O bands due to clay overlap C-O bands in the cellulose in the 1200-1000 cm^{-1} region (Jia *et al.*, 2011). The peaks at 998.18 and 910.42 cm^{-1} are also shifted to 993.36 and 909.45 cm^{-1} respectively in the nanocomposite, indicating a shift in Si-O-Mg and Al-Al-OH structures, respectively, due to cellulose incorporation into clay layers. These findings indicate strong interactions between the cellulose and the clay interlayers.

3.1.2 Characterization by Scanning Electron Microscopy

The morphology of clay, water hyacinth cellulose and clay-cellulose nanocomposite as observed by SEM, is shown in **Figure 2 (a, b** and **c).**

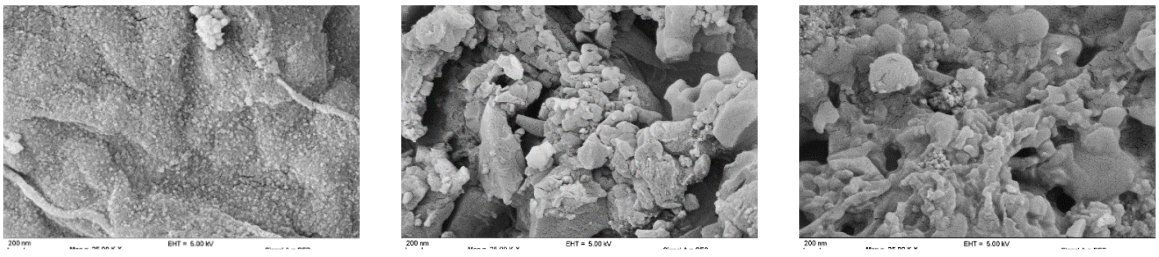

(a) (b) (c)

Figure 2: SEM image of clay(a), water hyacinth cellulose (b) and clay-cellulose nanocomposite (c).

According to **Figures 2**, the effect of incorporation of cellulose into the clay structure was seen to improve the surface porosity, thus increasing the surface area of the nanocomposite. Clay (**Figure 2a**) was seen to have a much smoother surface in comparison to the nanocomposite (**Figure 2c**). The increased porosity observed in the nanocomposite was responsible for providing more adsorptive

surface for the metal ions removal from contaminated water. Similar findings were reported by Soltani *et al.* (2019) who reported increased porosity in a polyaniline clay nanocomposite after incorporation of the polymer.

3.2 Optimization of Experimental Parameters

3.2.1 Effect of pH on Adsorption

In the current investigation, the effect of pH on the adsorption of Pb (II) and Cd (II) ions onto the clay-cellulose nanocomposite is illustrated in **Figure 4**, with an initial concentration of metal ions of 100 mg/L, adsorbent dose of 0.8 g, contact time 0f 120 minutes, shaken at 170 rpm.

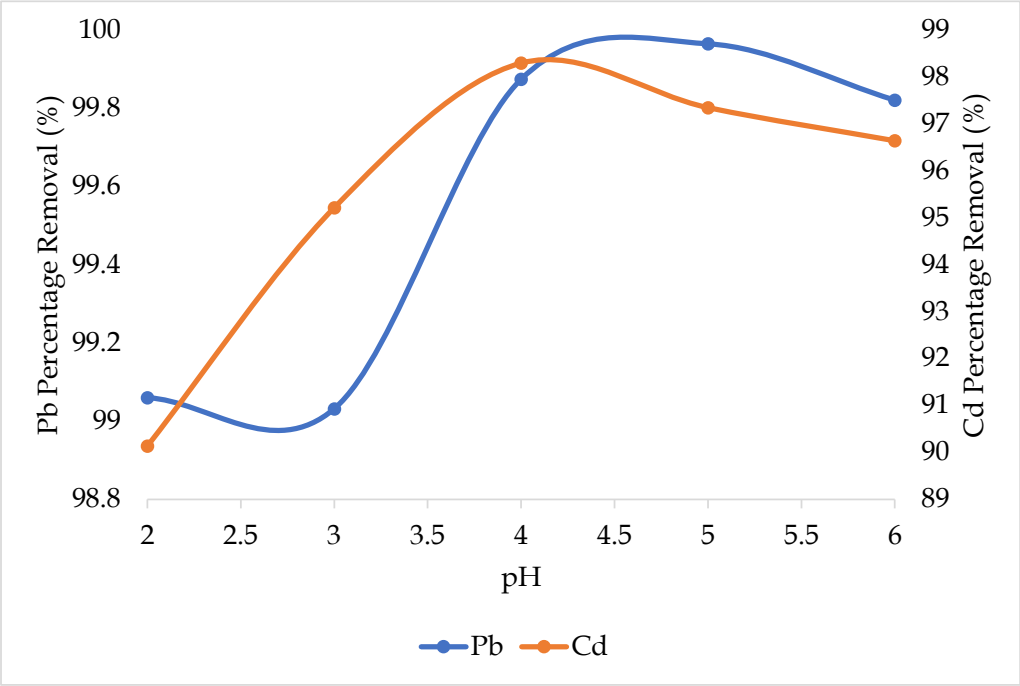

Figure 1: Effect of pH on the adsorption of Pb (II) and Cd (II) ions.

At low pH, the H^+ in the solution is highly dissociated and therefore competes for adsorptive sites on the adsorbent material. In this manner, metal ions tend to have low adsorption rates at low pH, which increases to a certain point and then deprecates again. Increase in pH towards alkalinity is associated with metal ion precipitation. At low pH, the nanocomposite exhibited a relatively low adsorption for Pb (II) ions and much lower for Cd (II). An increase in pH had a gradual increase in adsorption of the metal ions up to pH 4 for Cd (II) ions and Pb (II) ions, achieving 98.3% and 99.8% percentage removal, respectively, at equilibrium. The findings for Pb (II) ions adsorption are in agreement with Putro *et al.* (2017), who reported the highest adsorption of lead ions onto nanocrystalline cellulose bentonite nanocomposite at pH 5. Kanchana *et al.* (2012) observed a similar trend of metal ion adsorption with increasing pH in chitosan-based adsorbent where increasing pH from 4 to 8 had the highest adsorption of the Pb (II) ion at pH 6. Abunah *et al.*, (2019) reported data in agreement with Cd (II) ion adsorption, reporting the highest removal at a pH of 4.

3.2.2 Effect of Adsorbent Dosage

Effect of the dosage of the adsorbent on the adsorption of Pb (II) and Cd (II) ions at 25 °C, pH 4, contact time 120 minutes, and initial metal ion concentration 100 mg/L is illustrated in **Figure 5**. Increasing the adsorbent dose gradually increases the metal ion adsorption up to a certain point beyond which adsorption stabilizes or decreases. The initial gradual increase in metal ion adsorption is

attributed to the increase in adsorption sites with increase in adsorbent dosage. However, at higher doses, addition of the adsorbent onto the solution has no increase in adsorption due to depletion of adsorbable ions in the solution (Saber-Samandari *et al.*, 2016). In some instances, an increase in adsorbent mass has a decrease in adsorption of metal ions due to agglomeration of nanoparticles (Razzaz *et al.*, 2016). In the current research, the adsorption of 0.2, 0.8, 1.4, 2.0 and 2.6 g of nanocomposite mass was studied against the adsorption of lead and cadmium ions. The findings are presented in **Figure 5**.

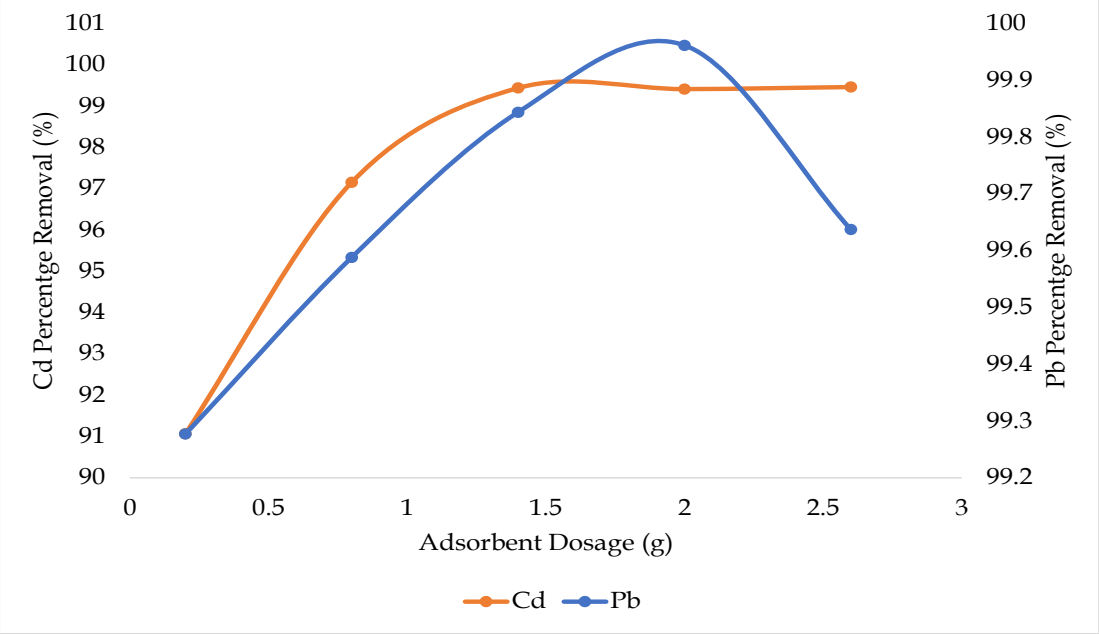

Figure 2: Effect of adsorbent dosage on adsorption of Pb (II) and Cd (II) ions

Increase in adsorption dosage had a gradual increase in adsorption of Cd (II) ions up to 1.4g beyond which adsorption slowed down. This is due to the depletion of adsorbates in the solution, and therefore a further increase in the adsorbate dose did not result in a large increase in adsorption (Fosso-Kankeu *et al.*, 2017). Similarly in the case of Pb (II) ion adsorption, the nanocomposite exhibited very high (99.28 %) initial adsorption of the metal ions even at small masses, which increased gradually up to 2.0 g of the nanocomposite, achieving 99.96 % removal, then decreased. Several factors could have contributed to this behavior inclusive of surface saturation, aggregation, diffusion limitations and hindered mass transfer. Initially, when the adsorbent dosage is low, the available surface area of the clay-cellulose nanocomposite is not fully utilized, and there are plenty of active sites available for metal ions to adsorb (Fosso-Kankeu *et al.*, 2017). As the dosage increases, more active sites become accessible, leading to increased adsorption. However, beyond a certain point, as the adsorbent dosage continues to increase, the particles may start to aggregate or form clusters (Ramkumar *et al.*, 2021). This aggregation reduces the accessibility of active sites for metal ions and restricts their diffusion through the adsorbent matrix, limiting further adsorption. This was well observed for Cd (II) ion adsorption, beyond 1.4 g of the nanocomposite. As the adsorbent dosage increases further, the distance between the active sites and the bulk solution increases due to the increased thickness of the adsorbent layer (Nasir *et al.*, 2019). This leads to an increase in the mass transfer resistance, making it harder for Pb (II) ions to reach the active sites on the surface of the adsorbent. Consequently, the overall adsorption efficiency decreases. The current findings are in agreement with other studies (Fosso-Kankeu *et al.*, 2017; Abunah *et al.*, 2019).

3.2.3 Effect of Initial Metal Ion Concentration

The effect of ion metal concentration at an adsorbate dosage of 1.4g, pH 4, contact time 120 minutes, temperature 25 °C and initial metal ion concentrations 10, 20, 30, 50, 100 mg/L is shown in **Figure 6**.

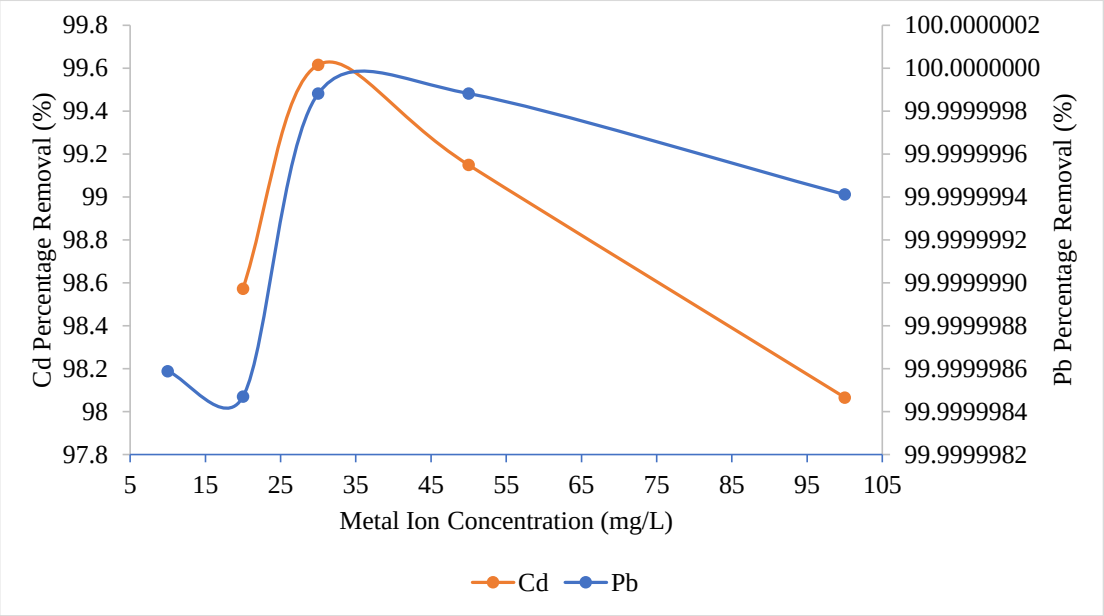

Figure 3: Effect of initial metal ion concentration.

A low initial concentration of metal ions is associated with low adsorption. Increasing the concentration of metal ions increases adsorption up to a certain point beyond which the adsorption decreases (Fosso-Kankeu *et al.*, 2017). This occurs as a result of the flooding of adsorbate ions for an unchanging number of active sites on the adsorbent. In **Figure 6**, it is observed that both Pb (II) and Cd (II) ion adsorption reached optimal at a relatively low initial metal ion concentration of 30 mg/L. Beyond this concentration, the adsorption deprecated steadily. This was because with high initial metal ion up take, most active sites of adsorption on the adsorbent became saturated, thus blocking further adsorption with increasing metal ion concentration (Abunah *et al.*, 2021). Similar trends for Pb (II) and Cd (II) ion adsorption with increasing concentration are reported by Hua & Li (2014) and Rao *et al.* (2010) using magnetized sulfhydryl functionalized hydrogel for Pb (II) removal and *Foeniculum vulgari* biomass for adsorption of Cd (II) ions, respectively.

3.2.4 Effect of Contact Time

The effect of contact time (10, 20, 30, 60 and 90 minutes) on the adsorption of Pb (II) and Cd (II) ions at a pH of 4, adsorbent dosage of 1.4 g (Cd) and 2.0 g(Pb), temperature of 25 °C, and initial metal ion concentration of 30 mg/L is given in **Figure 7**. In **Figure 7**, it was observed that the nanocomposite material adsorbed both Pb (II) Cd (II) ions drastically up to the 30^{th} and 20^{th} minutes respectively, beyond which a state of equilibrium was achieved. In the case of Pb (II) ion adsorption, the adsorbent material may not have fully equilibrated with the lead ions in the solution. At the beginning of the adsorption process, there may be a rapid initial uptake of metal ions due to the availability of vacant adsorption sites on the adsorbent surface (Inyinbor *et al.*, 2016). As the contact time increases from 10 to 20 minutes, the adsorbent sites might have been partially occupied, leading to a slight decrease in the rate of adsorption. As the contact time progresses beyond the initial phase, more metal ions have the opportunity to interact with the adsorbent surface. In the instance of Pb (II)

ions, the adsorption sites that were initially occupied may become desorbed or replaced by lead ions with a higher affinity for the surface (Ramkumar *et al.*, 2021). This can result in increased adsorption and a more efficient utilization of available adsorption sites. Additionally, during this period, the diffusion of metal ions into the internal structure of the adsorbent might take place, allowing for more complete interaction and adsorption. After a certain point, the adsorption process reaches a state of equilibrium where the rate of adsorption and desorption become balanced. At this stage, the adsorption capacity becomes relatively constant as the number of vacant adsorption sites decreases, and the overall metal concentration in the solution remains relatively unchanged. Therefore, from 30 to 60 minutes, the metal ion adsorption reaches a plateau, indicating that equilibrium has been reached. Similar adsorption trends were reported by Abunah *et al.* (2019) and Jiang *et al.* (2010).

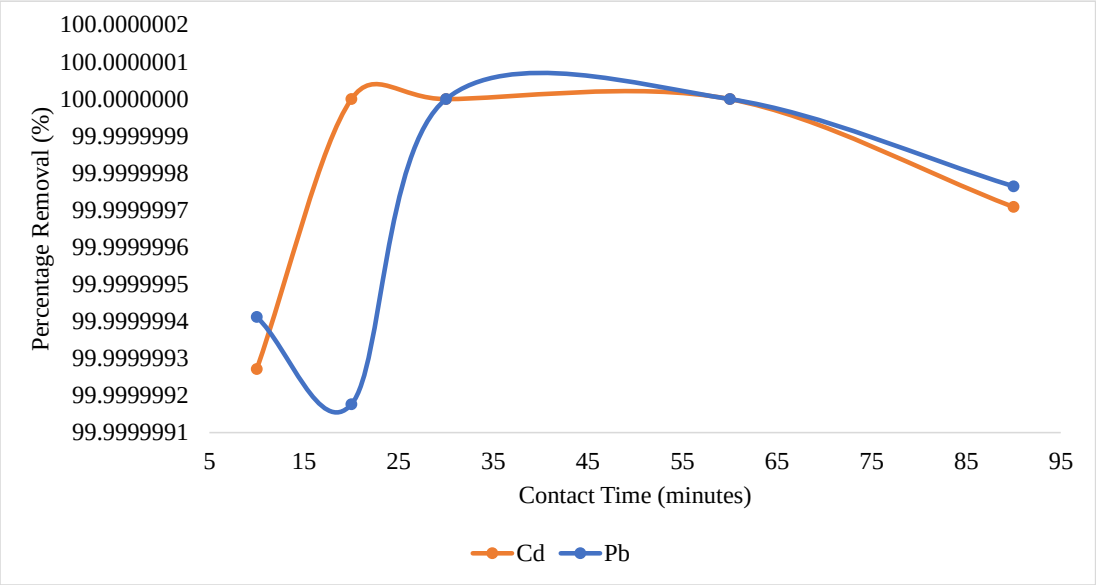

Figure 4: Effect of contact time on adsorption of Pb (II) and Cd (II) ions.

3.2.5 Effect of Temperature

The effect of temperature (20, 25, 30, 35 and 40 °C) on the adsorption of lead and cadmium ions is shown in **Figure 8** under shaking conditions with adsorbent dose of 0.8 g (Cd) and 2.0 g (Pb), pH 4, 30 mg/L metal ion concentration contact time 60 minutes and 170 rpm. According to **Figure 8**, Pb (II) ion adsorption was observed to initially decrease in removal with increase in temperature up to 25 °C, beyond which percentage removal increased to 35 °C. This trend implied a possible endothermic mechanism of adsorption. Endothermic adsorption is a common indicator if chemical adsorption whereby a metal ion is expected to be removed from the solution through chemical bonds with the adsorbent. Adsorption increases with increase in temperature since more energy is required to attach the ion to the adsorbent. However, at higher temperatures (beyond 35 °C in this case) it seems that the energy provided is strong enough to detach the ions from the adsorbent's surface, thereby a decrease in adsorption is observed. A similar trend of adsorption was reported by Hızal & Yılmazoğlu (2021, Azzaoui et al 2023). The adsorption of Cd (II) ions follows an opposite trend to Pb (II), whereby there was an initial increase in adsorption up to 25 °C, beyond which adsorption reduced gradually. The initial increase in adsorption with increase in temperature can be attributed to the need for activation energy for metal ion adsorption, although seemingly low for this case. Further increase in temperature contributed to a decrease in adsorption. This implied an exothermic adsorption process. Temperature affects adsorption depending on the nature of interaction between the adsorbate and the adsorbent.

Therefore, an increase in temperature can either decrease or increase adsorption of the metal ion depending on whether the adsorption process is exothermic or endothermic (Munagapati *et al.*, 2010).

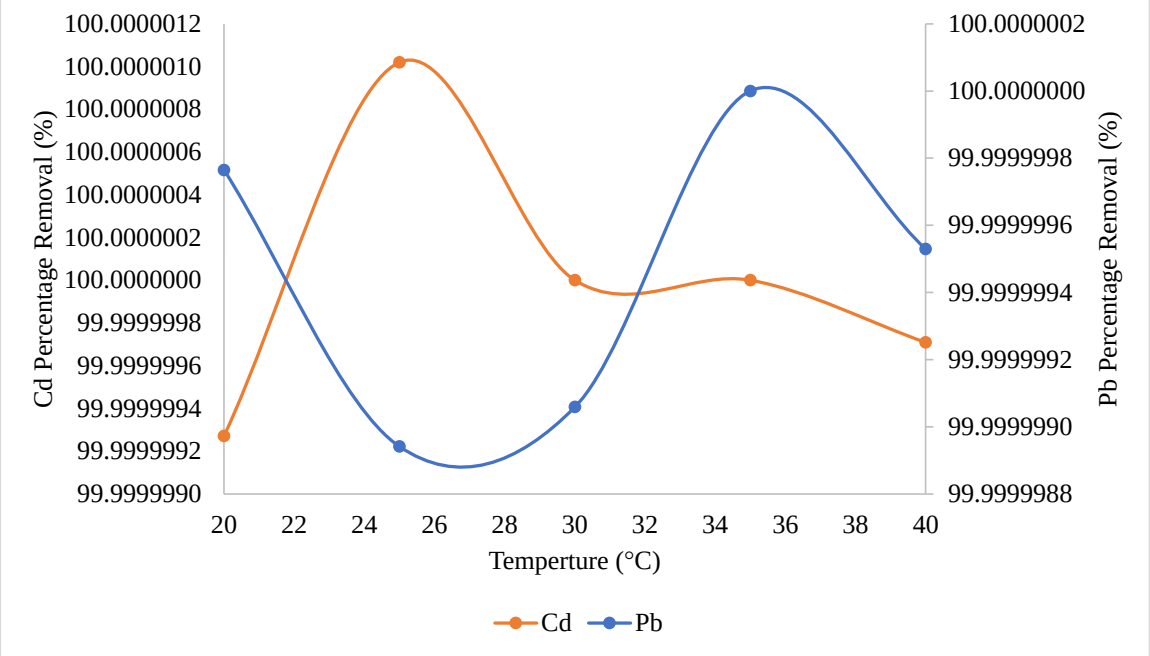

Figure 5: Effect of temperature on the adsorption of lead and cadmium ions.

An exothermic adsorption process will cause a decrease in metal ion adsorption with increase in temperature while an endothermic adsorption mechanism will cause an increase in adsorption with temperature increase (Fil, 2016). The effect on exothermic adsorption occurs due to increased ion mobility with increase in temperature. The ions gaining energy from higher temperature vibrate more rapidly to break the van der Waals forces attaching them to the adsorbate and therefore lower adsorption capacity is recorded with increase in temperature (P. Saha & Chowdhury, 2011). In this regard, exothermic adsorption is associated with physisorption.

3.3 Adsorption Studies

3.3.1 Thermodynamic Studies

Thermodynamic studies were conducted between the temperature range 298 – 318 K, with the goal of predicting the Gibbs free energy of adsorption, enthalpy, and entropy. The thermodynamic parameters are presented in **Table 1**. Gibbs free energy of adsorption was calculated from **Eqn. 15**, while enthalpy and entropy were calculated from the slope and intercept of the Van't Hoff plots respectively, using **Eqn. 16** (Yousefzadeh *et al.*, 2018). The values of Gibbs free energy give insight into the spontaneity of the adsorption process. According to **Table 1**, the adsorption of both Pb (II) and Cd (II) ions showed a negative Gibb's free energy for all the studied temperatures which indicated a spontaneous adsorption mechanism (Fosso-Kankeu *et al.*, 2017). This implies that adsorption is feasible at any temperature. The negative values of enthalpy indicated an exothermic adsorption process by nature (P. Saha & Chowdhury, 2011). From **Table 1**, the absolute enthalpy values for Pb (II) and Cd (II) are 170.059 kJ/mol and 7.368 kJ/mol. Since physisorption requires little energy to initiate the adsorption of a metal ion onto the adsorbent, the related enthalpy values are usually much lower, below 40 kJ/mol (Escudero *et al.*, 2016). In this regard, the value of the absolute enthalpy of Cd (II) ions implies a physisorption mechanism of removal. Pb (II) ions on the hand have an absolute enthalpy value in the range of physicochemical adsorption (below 240kJ/mol).

Table 1: Thermodynamic Parameters of Adsorption of Pb (II) and Cd (II) Ions

Adsorbent	Adsorbate	T (K)	ΔG° (kJ/mol)	ΔH° (kJ/mol)	ΔS° (J/mol/K
Clay cellulose nanocomposite	Pb (II)	298	-7.086	-170.059	-421.785
		308	-7.194		
		318	-6.805		
	Cd (II)	298	-1.311	-7.368	-20.144
		308	-1.278		
		318	-0.901		

The value is high since much more energy is required to make a chemical bond than a physical bond (Abunah *et al.*, 2021). The negative values of entropy calculated indicated less randomness at the adsorption interface between the solid/liquid interface. The decrease in randomness is attributed to the formation of an activated complex between the metal ion (adsorbate) and the nanocomposite (adsorbent). This implies associative adsorption that does not cause significant alteration of the internal structure of the adsorbent (P. Saha & Chowdhury, 2011).

3.3.2 Adsorption Isotherms

To gain more understanding on the mechanism of adsorption based on adsorbate concentration, Langmuir, Dubinim-Radushkevich, Temkin and Freundlich isotherm models were used. The linear fits of these isotherm models on Pb (II) and Cd (II) ion adsorption and their computed terms are given in **Figures 11, 12** and **Table 2** respectively.

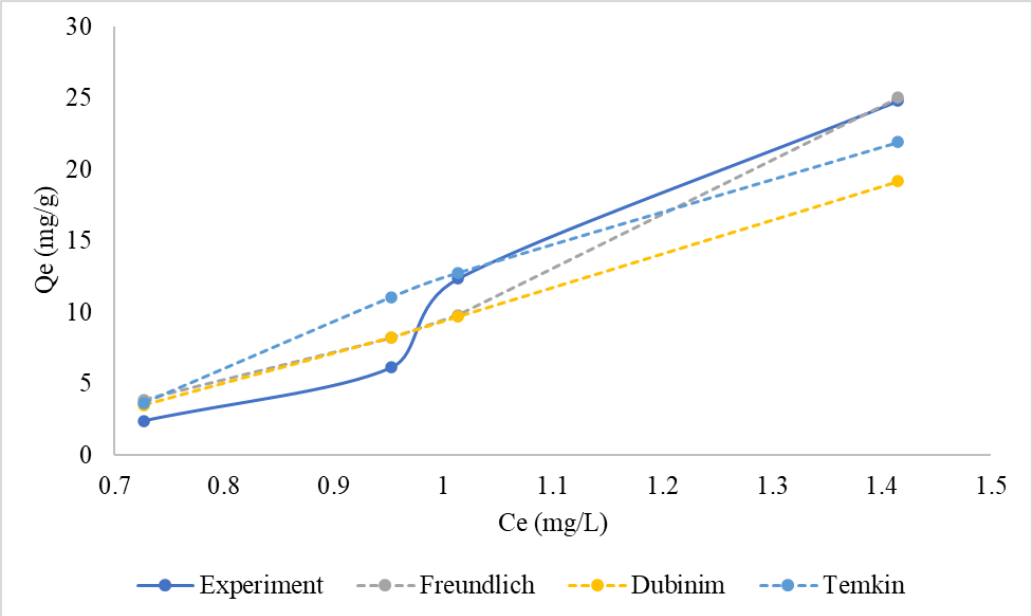

Figure 6: Pb (II) adsorption isotherm fits.

According to **Table 2**, Cd (II) adsorption was best described by Freundlich isotherm of all the isotherms it was fitted. This showed that it followed heterogenous adsorption process. Furthermore, the correlation to Langmuir isotherm also showed a high R^2 value of 0.9453, which showed that monolayer adsorption also took place in the adsorption of Cd (II) ions. From the literature, the value of n in Freundlich isotherm can provide insight on the type of adsorption that occurred.

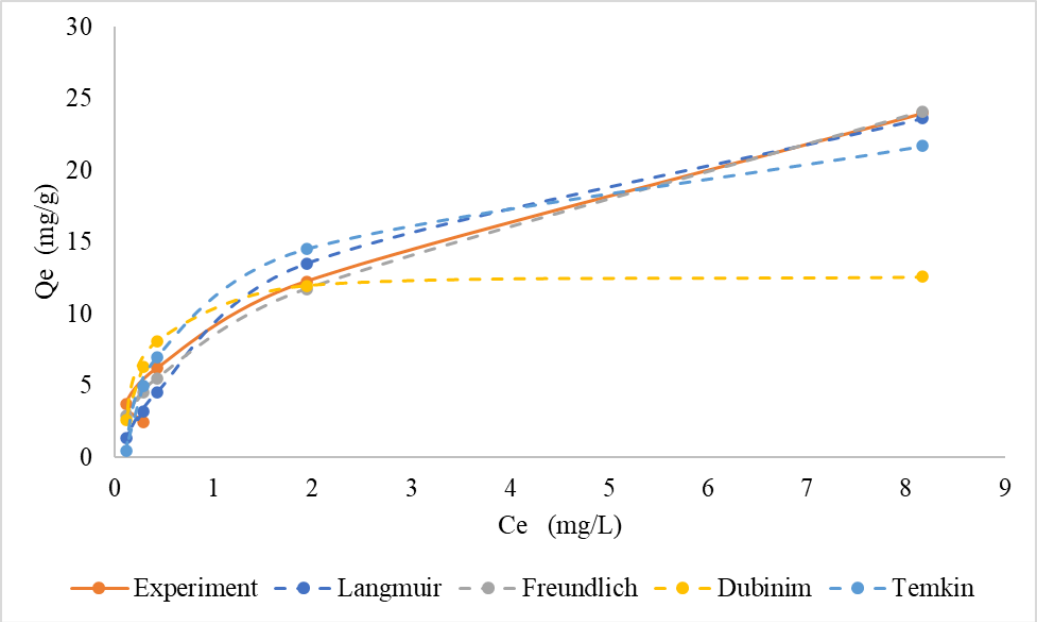

Figure 7: Cd (II) adsorption isotherm fits.

Table 2: Adsorption Isotherm Model Term Derivations

Adsorbent	Isotherm Model		Pb (II)	Cd (II)
Clay Cellulose Nanocomposite	Langmuir Isotherm	Qmax (mg/g)	-	30.79
		K_l	-	0.40
		R^2	-	0.9453
	Freundlich Isotherm	K_f	9.438	8.4351
		n	0.055	1.9999
		R^2	0.9444	0.9706
	Temkin Isotherm	b (J/mol)	90.349	496.756
		Kt (L/g)	0.571	9.509
		R^2	0.8124	0.8558
	Dubinim-Radushkevich Isotherm	Q_o (mg/g)	55.00	12.6177
		β	0.0000006	0.00000005
		E (kJ/mol)	0.9	3.1
		R^2	0.8150	0.2283

The cadmium (II) ion showed an n value above 1, indicating that the binding forces of the ion to the clay cellulose nanocomposite are principally physical forces, viz. van der Waals forces. This is supported by the value E in Dubinim-Radushkevich which is 3.1 kJ/mol, and the thermodynamic

studies previously discussed. Values of E below 8 kJ/mol imply a physisorption process, according to Matouq *et al.* (2015). From the Temkin isotherm, it is observed that both lead and cadmium have positive values of b. The term b refers to the heat of adsorption and, therefore, a positive value of b implies an exothermic adsorption process (Inyinbor *et al.*, 2016). This information agrees with the thermodynamic studies of the adsorption of Pb (II) and Cd (II) ions by the clay cellulose nanocomposite in this study. Freundlich's isotherm best described Pb (II) ion adsorption with an R^2 factor of 0.9444. This showed that the ion's adsorption was best describable as heterogenous. In addition, the value of n is very close to 0 compared to that of Cd (II) adsorption. This implies a highly heterogeneous nature of adsorption of the ion into the nanocomposite (Inyinbor *et al.*, 2016).

Conclusion

From the study of the adsorption of Pb (II) and Cd (II) ions by clay cellulose adsorption reported, it can be concluded that clay cellulose nanocomposite is efficient in adsorption of Pb (II) and Cd (II) ions with percentage removal ranging 98-99.6%. The most favorable parameters for the adsorption of Pb (II) and Cd (II) ions from wastewater are a pH of 4, an adsorbent dose of 0.8g per 100 ml of contaminated water, a temperature of 25 °C, and a contact time of 30 – 120 minutes. The adsorption of Pb (II) ions onto the clay-cellulose nanocomposite is best fitted to the Freundlich adsorption isotherm, which means that it underwent a heterogeneous adsorption process. Cd (II) ion adsorption followed both homogeneous and heterogeneous adsorption according to the adsorption isotherms, but was more correlated to the heterogeneity. The adsorption of both Pb (II) and Cd (II) ions was an exothermic process that was feasible at any temperature.

Acknowledgement: The authors acknowledge Kenya Forestry Research Institute for providing access to Atomic Absorption Spectroscopy services, the Department of Chemistry, Kenyatta University for providing access to Fourier Transform Infrared Spectrometer and Instituto de Ciencias de la Construcción Eduardo Torroja (CSIC) for Scanning Electron Microscopy Imaging**.**

Disclosure statement: *Conflict of Interest:* The authors declare that there are no conflicts of interest. *Compliance with Ethical Standards:* This article does not contain any studies involving human or animal subjects.

References

Aaddouz M; Azzaoui K; Akartasse N; Mejdoubi E; Hammouti B; Taleb M; Sabbahi R; Alshahateet S.F. (2023). Removal of methylene blue from aqueous solution by adsorption onto hydroxyapatite nanoparticles. *Journal of Molecular Structure*. 1288(15), 135807. https://doi.org/10.1016/j.molstruc.2023.135807

Abunah, D., Onindo, C., & Andala, D. (2021). Physico-chemical removal of cu (II) and cd (II) ions from contaminated water using recyclable montmorillonite-cellulose nanocomposite [Thesis, Kenyatta University]. http://ir-library.ku.ac.ke/handle/123456789/22655

Abunah, D., Onindo, C., Andala, D., & Ochoti, E. (2019). Physico-chemical removal of heavy metals from contaminated water using recyclable montmorillonite cellulose nanocomposite. *Journal of Materials and Environmental Sciences*, 10(12), 1349–1361. http://www.jmaterenvironsci.com/Document/vol10/vol10_N12/JMES-2019-10-133-Abunah.pdf

Alexander, J. A., Ahmad Zaini, M. A., Abdulsalam, S., El-Nafaty, U. A., & Aroke, U. O. (2018). Physicochemical characteristics of surface modified Dijah-Monkin bentonite. *Particulate Science and Technology*, 36(3), 287–297. https://doi.org/10.1080/02726351.2016.1245689

Aloulou, W., Aloulou, H., Khemakhem, M., Duplay, J., Daramola, M. O., & Ben Amar, R. (2020). Synthesis and characterization of clay-based ultrafiltration membranes supported on natural zeolite for removal of heavy metals from wastewater. *Environmental Technology and Innovation*, 18, 100794. https://doi.org/10.1016/j.eti.2020.100794

Alsawalha, M., Obra, E. C., & Salman Al-Odah, H. (2016). FT-IR and SEM studies on natural clays. IRES International Conference, 1–5.

Altaher, H. (2016). What is the significance of Temkin parameters in adsorption of metal? Research Gate. https://www.researchgate.net/post/What_is_the_significance_of_Temkin_parameters_in_adsorption_of_metal

Apanpa-Qasim, A. F. I., Adeyi, A. A., Mudliar, S. N., Raghunathan, K., & Thawale, P. (2016). Examination of Lead and Cadmium in Water-based Paints Marketed in Nigeria. *Journal of Health and Pollution*, 6(12), 43–49. https://doi.org/10.5696/2156-9614-6.12.43

Akartasse, N., Azzaoui, K., Mejdoubi, E., Lhaj Lahcen Elansari, Hammouti, B., Siaj, M., Jodeh, S., Hanbali, G., Hamed, R., and Rhazi. L. (2022). Chitosan-Hydroxyapatite Bio-Based Composite in Film Form: Synthesis and Application in Wastewater. *Polymers* 14, 20, 4265. https://doi.org/10.3390/polym14204265

Arya, V., & Materials, L. P. (2016). Adsorption of pharmaceuticals in water using Fe3O4 coated polymer clay composite. Elsevier. https://www.sciencedirect.com/science/article/pii/S1387181116302359

Ashouri, M. Z., Hayati-Ashtiani, M., & Rezaei, M. (2021). Adsorption of nickel from aqueous solutions by natural and acid-activated nano-structured bentonite. *Particulate Science and Technology*, 1–7. https://doi.org/10.1080/02726351.2021.1998269

Ayawei, N., Ebelegi, A. N., & Wankasi, D. (2017). Modelling and Interpretation of Adsorption Isotherms. *Journal of Chemistry*, 2017. https://doi.org/10.1155/2017/3039817

Azzaoui K.; Mejdoubi E; Lamhamdi A; Hammouti B; Akartasse N; Berrabah M; Elidrissi A; Jodeh S; Hamed O; Abidi N. (2016). Novel tricomponenets composites films from polylactic acid/ hydroxyapatite/ poly-caprolactone suitable for biomedical applications. *Journal of Materials and Environmental Science.* 7, (3), 761 – 769. ISSN 20282508

Azzaoui, K., Aaddouz, M., Akartasse, N. et al. (2023). Synthesis of β-Tricalcium Phosphate/PEG 6000 Composite by Novel Dissolution/Precipitation Method: Optimization of the Adsorption Process Using a Factorial Design—DFT and Molecular Dynamic. *Arab J Sci Eng* . https://doi.org/10.1007/s13369-023-08390-8

Azeh Engwa, G., Udoka Ferdinand, P., Nweke Nwalo, F., & N. Unachukwu, M. (2019). Mechanism and Health Effects of Heavy Metal Toxicity in Humans. In O. Karcioglu & B. Arslan (Eds.), Poisoning in the Modern World - New Tricks for an Old Dog? (1st ed., pp. 77–95). IntechOpen. https://doi.org/10.5772/intechopen.82511

Benkaddour R., Hammouti B., El-Mrabet M., Dahchour M., Aouniti A., Haouadi B., Ouardi A. (2004), Salinité et pollution par les nitrates des eaux souterraines de la plaine de Triffa, *Actes Inst. Agron. Vet. (Maroc)* 24N°3&4, 147-158.

Bruice, P. Y. (2016). The Intensity of Absorption Bands. In Organic Chemistry (pp. 1–13). https://chem.libretexts.org/Bookshelves/Organic_Chemistry/Map%3A_Organic_Chemistry_(Bruice)/13%3A_Mass_Spectrometry_Infrared_Spectroscopy_and_Ultraviolet_Visible_Spectroscopy/13.13%3A_The_Shape_of_Absorption_Bands

Chashechnikova, I., Dolgov, L., Gavrilko, T., Puchkovska, G., Shaydyuk, Y., Lebovka, N., Moraru, V., Baran, J., & Ratajczak, H. (2005). Optical properties of heterogeneous nanosystems based on montmorillonite clay mineral and 5CB nematic liquid crystal. *Journal of Molecular Structure*, 744–747(SPEC. ISS.), 563–571. https://doi.org/10.1016/J.MOLSTRUC.2004.11.047

Chu, K. H. (2021). Revisiting the Temkin Isotherm: Dimensional Inconsistency and Approximate Forms. *Industrial and Engineering Chemistry Research*, 60(35), 13140–13147. https://doi.org/10.1021/ACS.IECR.1C01788/ASSET/IMAGES/MEDIUM/IE1C01788_0007.GIF

Daumier, H., Savage, A., Sicyon, B. O., & Augustyn, A. (2020). *Clay. Encyclopedia Britannica.* https://www.britannica.com/science/clay-geology

El Kassimi, A., Achour, Y., El Himri, M., Laamari, R., & El Haddad, M. (2021). Removal of two cationic dyes from aqueous solutions by adsorption onto local clay: experimental and theoretical study using DFT method. *International Journal of Environmental Analytical Chemistry*, 101, 1–22. https://doi.org/10.1080/03067319.2021.1873306

El-Aziz, A. M. E., Kamal, K. H., Ali, K. A., Abdel-Aziz, M. S., & Kamel, S. (2018). Biodegradable grafting cellulose/clay composites for metal ions removal. *International Journal of Biological Macromolecules*, 118, 2256–2264. https://doi.org/10.1016/j.ijbiomac.2018.07.105

El Hammari L., Latifi S., Saoiabi S., Azzaoui K., Hammouti B., Chetouani A., Sabbahi R.. (2022). Toxic heavy metals removal from river water using a porous phospho-calcic hydroxyapatite. *Mor. J. Chem.* 10 (1), 062 – 072. https://doi.org/10.48317/IMIST.PRSM/morjchem-v10i1.31752

Escudero, J., Notario, B., Jimenez, C., & Rodriguez-Perez, M. A. (2016). Characterization of nanoclay intercalation during foaming with in situ energy-dispersive X-ray diffraction. *Journal of Applied Polymer Science*, 133(20). https://doi.org/10.1002/APP.43432

Fil, B. A. (2016). Isotherm, kinetic, and thermodynamic studies on the adsorption behavior of malachite green dye onto montmorillonite clay. *Particulate Science and Technology*, 34(1), 118–126. https://doi.org/10.1080/02726351.2015.1052122

Foo, K. Y., & Hameed, B. H. (2010). Insights into the modeling of adsorption isotherm systems. *Chemical Engineering Journal*, 156(1), 2–10. https://doi.org/10.1016/J.CEJ.2009.09.013

Fosso-Kankeu, E., Mittal, H., Waanders, F., & Ray, S. S. (2017). Thermodynamic properties and adsorption behaviour of hydrogel nanocomposites for cadmium removal from mine effluents. *Journal of Industrial and Engineering Chemistry*, 48, 151–161. https://doi.org/10.1016/J.JIEC.2016.12.033

Frogner-Kockum, P., Göransson, G., & Haeger-Eugensson, M. (2020). Impact of Climate Change on Metal and Suspended Sediment Concentrations in Urban Waters. *Frontiers in Environmental Science*, 8, 269. https://doi.org/10.3389/FENVS.2020.588335/BIBTEX

Gaffney, J. S., Marley, N. A., & Jones, D. E. (2012). Fourier Transform Infrared (FTIR) Spectroscopy. In Characterization of Materials (Vol. 10, Issue 8, p. 191). John Wiley & Sons, Inc. https://doi.org/10.1002/0471266965.com107.pub2

Gu, S., Kang, X., Wang, L., Lichtfouse, E., & Wang, C. (2019). Clay mineral adsorbents for heavy metal removal from wastewater: a review. *Environmental Chemistry Letters*, 17(2), 629–654. https://doi.org/10.1007/s10311-018-0813-9

Hayati-Ashtiani, M. (2012). Use of FTIR Spectroscopy in the Characterization of Natural and Treated Nanostructured Bentonites (Montmorillonites). Particulate Science and Technology, 30(6), 553–564. https://doi.org/10.1080/02726351.2011.615895

Hızal, J., & Yılmazoğlu, M. (2021). Montmorillonite Clay Composite for Heavy Metal Removal from *Water*. 93–112. https://doi.org/10.1007/978-3-030-47400-3_4

Hua, R., & Li, Z. (2014). Sulfhydryl functionalized hydrogel with magnetism: Synthesis, characterization, and adsorption behavior study for heavy metal removal. *Chemical Engineering Journal*, 249, 189–200. https://linkinghub.elsevier.com/retrieve/pii/S1385894714003866

Imam, D. M., Rizk, S. E., & Attallah, M. F. (2020). Adsorption studies of Ce(III) and Zr(IV) from aqueous solution using clay and humic acid—clay materials. *Particulate Science and Technology*, 38(8), 922–930. https://doi.org/10.1080/02726351.2019.1636914

Inyinbor, A. A., Adekola, F. A., & Olatunji, G. A. (2016). Kinetics, isotherms and thermodynamic modeling of liquid phase adsorption of Rhodamine B dye onto Raphia hookerie fruit epicarp. *Water Resources and Industry*, 15, 14–27. https://doi.org/10.1016/j.wri.2016.06.001

Iordache, A. M., Nechita, C., Voica, C., Pluháček, T., & Schug, K. A. (2022). Climate change extreme and seasonal toxic metal occurrence in Romanian freshwaters in the last two decades—case study and critical review. *Npj Clean Water* 5:1, 5(1), 1–9. https://doi.org/10.1038/s41545-021-00147-w

Istirokhatun, T., Rokhati, N., Rachmawaty, R., Meriyani, M., Priyanto, S., & Susanto, H. (2015). Cellulose Isolation from Tropical Water Hyacinth for Membrane Preparation. *Procedia Environmental Sciences*, 23, 274–281. https://doi.org/10.1016/j.proenv.2015.01.041

Jia, N., Li, S. M., Ma, M. G., Zhu, J. F., & Sun, R. C. (2011). Synthesis and characterization of cellulose-silica composite fiber in ethanol/water mixed solvents. *BioResources*, 6(2), 1186–1195.

Jiang, M. qin, Jin, X. ying, Lu, X. Q., & Chen, Z. liang. (2010). Adsorption of Pb(II), Cd(II), Ni(II) and Cu(II) onto natural kaolinite clay. Desalination, 252(1–3), 33–39. https://doi.org/10.1016/J.DESAL.2009.11.005

Jodeh, S., Hamed, O., Melhem, A., Salghi, R., Jodeh, D., Azzaoui, K., Benmassaoud, Y., (...), Murtada, K. (2018) .Magnetic nanocellulose from olive industry solid waste for the effective removal of methylene blue from wastewater. *Environmental Science and Pollution Research*, 25 (22), 22060-22074. https://doi.org/10.1007/s11356-018-2107-y

Juve, J.-M. A., Christensen, F. M. S., *et al.* (2022). Electrodialysis for metal removal and recovery: A review. *Chemical Engineering Journal*, 435, 134857. https://doi.org/10.1016/j.cej.2022.134857

Kanchana, V., Gomathi, T., Geetha, V., & Sudha, P. N. (2012). Adsorption analysis of pb(II) by nanocomposites of chitosan with methyl cellulose and clay. *Der Pharmacia Lettre*, 4(4), 1071–1079.

Karunakaran, A., Chaturvedi, A., Ali, J., Singh, R., Agarwal, S., & Garg, M. C. (2021). Response surface methodology-based modeling and optimization of chromium removal using spiral-wound reverse-osmosis membrane setup. *International Journal of Environmental Science and Technology* 2021, 1–12. https://doi.org/10.1007/S13762-021-03422-Y

Kennedy, K. K., Maseka, K. J., Mbulo, M., Kennedy, K. K., Maseka, K. J., & Mbulo, M. (2018). Selected Adsorbents for Removal of Contaminants from Wastewater: Towards Engineering Clay Minerals. *Open Journal of Applied Sciences*, 8(8), 355–369. https://doi.org/10.4236/OJAPPS.2018.88027

Kumar, A. S. K., Kalidhasan, S., Rajesh, V., & Rajesh, N. (2012). Application of Cellulose-Clay Composite Biosorbent toward the Effective Adsorption and Removal of Chromium from Industrial Wastewater. *Industrial & Engineering Chemistry Research*, 51(1), 58–69. https://doi.org/10.1021/ie201349h

Kuwonu, F. (2017). Urban growth a boon for Africa's industrialization. *Africa Renewal*, 31(1), 14–15. https://doi.org/10.18356/cdedc973-en

Malone, M. O. (2016). Half the World to Face Severe Water Stress by 2030 unless Water Use is "Decoupled" from Economic Growth, Says International Resource Panel. In UNEP - UN Environment Programme. https://www.unep.org/news-and-stories/press-release/half-world-face-severe-water-stress-2030-unless-water-use-decoupled

Marshall, K. (2017). Cost of Industrial Water Treatment System. https://www.samcotech.com/how-much-does-an-industrial-water-treatment-system-cost/

Matouq, M., Jildeh, N., Qtaishat, M., Hindiyeh, M., & Al Syouf, M. Q. (2015). The adsorption kinetics and modeling for heavy metals removal from wastewater by Moringa pods. *Journal of Environmental Chemical Engineering*, 3(2), 775–784. https://doi.org/10.1016/J.JECE.2015.03.027

Megertu, D. G., & Bayissa, L. D. (2020). Heavy metal contents of selected commercially available oil-based house paints intended for residential use in Ethiopia. *Environmental Science and Pollution Research*, 27(14), 17175–17183. https://doi.org/10.1007/S11356-020-08297-Z

Mu, T.-H., & Sun, H.-N. (2019). Sweet Potato Leaf Polyphenols: Preparation, Individual Phenolic Compound Composition and Antioxidant Activity. *Polyphenols in Plants*, 365–380. https://doi.org/10.1016/B978-0-12-813768-0.00022-0

Munagapati, V. S., Yarramuthi, V., Nadavala, S. K., Alla, S. R., & Abburi, K. (2010). Biosorption of Cu(II), Cd(II) and Pb(II) by Acacia leucocephala bark powder: Kinetics, equilibrium and thermodynamics. *Chemical Engineering Journal*, 157(2–3), 357–365. https://doi.org/10.1016/J.CEJ.2009.11.015

Nasir, A. M., Goh, P. S., Abdullah, M. S., Ng, B. C., & Ismail, A. F. (2019). Adsorptive nanocomposite membranes for heavy metal remediation: Recent progresses and challenges. *Chemosphere*, 232, 96–112. https://doi.org/10.1016/J.CHEMOSPHERE.2019.05.174

Neitzel, I., Mochalin, V., & Gogotsi, Y. (2012). Advances in Surface Chemistry of Nanodiamond and Nanodiamond–Polymer Composites. In Ultananocrystalline Diamond (Vol. 1, pp. 421–456). Elsevier. https://doi.org/10.1016/B978-1-4377-3465-2.00013-X

Nelligan, T. (Environment A. and S.D., Wirth, S. (Business S.M.D., Cuypere, C.D. (Environment A. and S.D., & Mach, L. (Social S.M.D. (2011). Operation and maintenance costs of drinking water plants. *Operational Geographer*, 9(1), 9–13. https://www150.statcan.gc.ca/n1/pub/16-002-x/2011001/part-partie3-eng.htm

NIH. (2021, March 22). Copper - Consumer Fact Sheet. U.S. Department of Health & Human Services. https://ods.od.nih.gov/factsheets/Copper-Consumer/

NIH. (2022, April 5). Iron - Consumer Fact Sheet. U.S. Department of Health & Human Services. https://ods.od.nih.gov/factsheets/Iron-Consumer/

Njuguna, S. M., Yan, X., Gituru, R. W., Wang, Q., & Wang, J. (2017). Assessment of macrophyte, heavy metal, and nutrient concentrations in the water of the Nairobi River, Kenya. *Environmental Monitoring and Assessment*, 189:9, 189(9), 1–14. https://doi.org/10.1007/S10661-017-6159-0

Ogilo, J. K., Onditi, A. O., Salim, A. M., & Yusuf, A. O. (2017). Assessment of Levels of Heavy Metals in Paints from Interior Walls and Indoor Dust from Residential Houses in Nairobi City County, Kenya. *Chemical Science International Journal*, 21(1), 1–7. https://doi.org/10.9734/CSJI/2017/37392

Ostovaritalab, M.-A. A., & Hayati-Ashtiani, M. (2019). Investigation of Cs(I) and Sr(II) removal using nanoporous bentonite. *Particulate Science and Technology*, 37(7). https://doi.org/10.1080/02726351.2018.1455779

Putro J.N., Santoso S.P., Ismadji S., Ju Y.H. (2017). Investigation of heavy metal adsorption in binary system by nanocrystalline cellulose – Bentonite nanocomposite: Improvement on extended Langmuir isotherm model. *Microporous and Mesoporous Materials*, 246, 166–177. https://doi.org/10.1016/j.micromeso.2017.03.032

Ramkumar, J., Majeed, J., & Chandramouleeswaran, S. (2021). Insight to sorption mechanism employing nanocomposite: Case study of toxic species removal. *Microporous and Mesoporous Materials*, 314, 110858. https://doi.org/10.1016/J.MICROMESO.2020.110858

Rao, R. A. K., Khan, M. A., & Rehman, F. (2010). Utilization of Fennel biomass (Foeniculum vulgari) a medicinal herb for the biosorption of Cd(II) from aqueous phase. *Chemical Engineering Journal*, 156(1), 106–113. https://doi.org/10.1016/J.CEJ.2009.10.005

Razzaz, A., Ghorban, S., Hosayni, L., Irani, M., & Aliabadi, M. (2016). Chitosan nanofibers functionalized by TiO_2 nanoparticles for the removal of heavy metal ions. *Journal of the Taiwan Institute of Chemical Engineers*, 58(58), 333–343. https://doi.org/10.1016/j.jtice.2015.06.003

Rehman K., Fatima F., Waheed I., & Akash M.S.H. (2018). Prevalence of exposure of heavy metals and their impact on health consequences. *Journal of Cellular Biochemistry*, 119(1), 157–184. https://doi.org/10.1002/jcb.26234

Razzouki, B. Azzaoui K; Errich A; Lamhamdi A. Berrabah M; Elansari L.L. (2015). Physicochemical study of arsenic removal using iron hydroxide. *Journal of Materials and Environmental Science*. 6 (5), 1444 – 1450

Saber-Samandari, S., Saber-Samandari, S., Heydaripour, S., & Abdouss, M. (2016). Novel carboxymethyl cellulose based nanocomposite membrane: Synthesis, characterization and application in water treatment. *Journal of Environmental Management*, 166, 457–465. https://doi.org/10.1016/J.JENVMAN.2015.10.045

Saha, D., & Grappe, H. A. (2017). Adsorption properties of activated carbon fibers. Activated Carbon Fiber and Textiles, 143–165. https://doi.org/10.1016/B978-0-08-100660-3.00005-5

Saha, P., & Chowdhury, S. (2011). Insight Into Adsorption Thermodynamics. *Thermodynamics*. https://doi.org/10.5772/13474

Sdiri, A., Higashi, T., Hatta, T., Jamoussi, F., & Tase, N. (2011). Evaluating the adsorptive capacity of montmorillonitic and calcareous clays on the removal of several heavy metals in aqueous systems. *Chemical Engineering Journal*, 172(1), 37–46. https://doi.org/10.1016/j.cej.2011.05.015

Soltani, H., Belmokhtar, A., Zeggai, F. Z., Benyoucef, A., Bousalem, S., & Bachari, K. (2019). Copper(II) Removal from Aqueous Solutions by PANI-Clay Hybrid Material: Fabrication, Characterization, Adsorption and Kinetics Study. *Journal of Inorganic and Organometallic Polymers and Materials*, 29(3), 841–850. https://doi.org/10.1007/S10904-018-01058-Z

Suhas, Gupta, V. K., Carrott, P. J. M., Singh, R., Chaudhary, M., & Kushwaha, S. (2016). Cellulose: A review as natural, modified and activated carbon adsorbent. *Bioresource Technology*, 216, 1066–1076. https://doi.org/10.1016/J.BIORTECH.2016.05.106

Tirtom, V. N., Dinçer, A., Becerik, S., Aydemir, T., & Çelik, A. (2012). Comparative adsorption of Ni(II) and Cd(II) ions on epichlorohydrin crosslinked chitosan–clay composite beads in aqueous solution. *Chemical Engineering Journal*, 197, 379–386. https://doi.org/10.1016/J.CEJ.2012.05.059

Tutic, A., Novakovic, S., Lutovac, M., Biocanin, R., Ketin, S., & Omerovic, N. (2015). The Heavy Metals in Agrosystems and Impact on Health and Quality of Life. *Open Access Macedonian Journal of Medical Sciences*, 3(2), 345. https://doi.org/10.3889/OAMJMS.2015.048

UN Water, (2021). Water Quality and Wastewater. United Nations. https://www.unwater.org/water-facts/quality-and-wastewater/

UNEP. (2020). How climate change is making record-breaking floods the new normal. United Nations. https://www.unep.org/news-and-stories/story/how-climate-change-making-record-breaking-floods-new-normal

UN-Water. (2018, March 19). World Water Development Report 2018. World Water Development Report. https://www.unwater.org/publications/world-water-development-report-2018/

Yeganeh, G., Ramavandi, B., Esmaeili, H., & Tamjidi, S. (2019). Dataset of the aqueous solution and petrochemical wastewater treatment containing ammonia using low cost and efficient bio-adsorbents. *Data in Brief*, 26, 104308. https://doi.org/10.1016/j.dib.2019.104308

Yildiz, N., Aktas, Z., & Calimli, A. (2004). Sulphuric Acid Activation of a Calcium Bentonite. *Particulate Science and Technology*, 22(1), 21–33. https://doi.org/10.1080/02726350490422392

Yousefzadeh, H., Salarian, A. A., & Sid Kalal, H. (2018). Study of Pb (II) adsorption from aqueous solutions by TiO_2 functionalized with hydroxide ethyl aniline (PHEA/n-TiO_2). *Journal of Molecular Liquids*, 263, 294–302. https://doi.org/10.1016/J.MOLLIQ.2018.03.023

Zhang, X., & Wang, X. (2015). Adsorption and desorption of Nickel(II) ions from aqueous solution by a lignocellulose/montmorillonite nanocomposite. *PLoS ONE*, 10(2), e0117077. https://doi.org/10.1371/journal.pone.0117077